

Article

The Microstructure of Nanocrystalline TiB₂ Films Prepared by Chemical Vapor Deposition

Xiaoxiao Huang, Shuchen Sun *, Ganfeng Tu, Shuaidan Lu, Kuanhe Li and Xiaoping Zhu

School of Metallurgy, Northeastern University, No. 3-11, Wenhua Road, Heping District, Shenyang 110819, China; huangxiaoxiao@outlook.com (X.H.); tugf@smm.neu.edu.cn (G.T.); imiage@163.com (S.L.); kevinlee579@outlook.com (K.L.); xiaopingzhu007@outlook.com (X.Z.)

* Correspondence: sunsc@smm.neu.edu.cn; Tel.: +86-024-8368-9195

Received: 7 November 2017; Accepted: 11 December 2017; Published: 13 December 2017

Abstract: Nanocrystalline titanium diboride (TiB₂) ceramics films were prepared on a high purity graphite substrate via chemical vapor deposition (CVD). The substrate was synthesized by a gas mixture of TiCl₄, BCl₃, and H₂ under 1000 °C and 10 Pa. Properties and microstructures of TiB₂ films were also examined. The as-deposited TiB₂ films had a nano-sized grain structure and the grain size was around 60 nm, which was determined by X-ray diffraction, field emission scanning electron microscopy, and transmission electron microscopy. Further research found that a gas flow ratio of TiCl₄/BCl₃ had an influence on the film properties and microstructures. The analyzed results illustrated that the grain size of the TiB₂ film obtained with a TiCl₄/BCl₃ gas flow ratio of 1, was larger than the grain size of the as-prepared TiB₂ film prepared with a stoichiometric TiCl₄/BCl₃ gas flow ratio of 0.5. In addition, the films deposited faster at excessive TiCl₄. However, under the condition of different TiCl₄/BCl₃ gas flow ratios, all of the as-prepared TiB₂ films have a preferential orientation growth in the (100) direction.

Keywords: TiB₂; nanocrystalline films; microstructure; chemical vapor deposition

1. Introduction

The titanium diboride (TiB₂) is an interesting and very useful ceramic material. It displays many attractive properties such as high melting temperature, high hardness, high elastic modulus, erosion resistance, excellent chemical stability, and good thermal as well as electrical conductivity [1–6]. Thus, TiB₂ is widely applied as the evaporator boat in high vacuum metal films, the protection of weapons and armored vehicle [7–9]. In addition, the neutron absorption of boron coupled with the above-high-temperature properties makes TiB₂ the best choice of control rod material for high-temperature nuclear reactors [10–12].

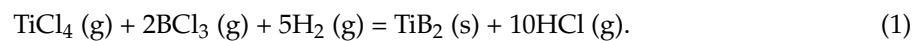
The outstanding properties of TiB₂ depend on its microstructure. TiB₂ crystallizes with a hexagonal structure with a P6/mmm space group [13,14]. Titanium atoms are located at the vertex of the hexagonal prism and the center of the bottom, boron atoms fill the trigonal prisms that are formed by the titanium atoms, and the boron atom and the titanium atom alternately form a 2D honeycomb network structure. B–B is covalently bonded, and B–Ti is bounded by ion bonds [15,16]. The lattice parameters of TiB₂ are as follows: $a = b = 3.029$, $c = 3.228$, $\alpha = \beta = \pi/2$, and $\gamma = \pi/3$ [17,18].

Over the past few decades, many studies have been carried out on the deposition of TiB₂ films by chemical vapor deposition (CVD) methods [19–21], plasma assisted chemical vapor deposition (PACVD) methods [6,11], and plasma enhanced chemical vapor deposition (PECVD) methods [22]. Takehiko Takahashi and Hideo Kamiya [21] investigated the influence of deposition temperature on the deposition phase using CVD methods, the results show that TiB₂ could be deposited above 800 °C. A. J. Caputo et al. [19] have researched the effect of deposition temperature on film hardness, the surface morphology of the films, and deposition rate via CVD methods. The PACVD and PECVD

technique have a low deposition temperature range of 250~650 °C. In this paper, nanocrystalline TiB₂ films on a high pure graphite substrate were deposited at a higher temperature (1000 °C) by a CVD system. The purpose of our work was to investigate the deposition results and to prepare for further study in which TiB₂ films are deposited on a nickel-based superalloy substrate. Because of the properties of nickel-based superalloys, deposition temperatures should not exceed 1000 °C. Thus, the deposition temperature was also limited to 1000 °C in this experiment. The structure of the TiB₂ films was examined by X-ray diffraction (XRD), field emission scanning electron microscopy (FESEM), transmission electron microscopy (TEM), and energy dispersive spectroscopy (EDS). Furthermore, the TiB₂ films were synthesized using different TiCl₄/BCl₃ gas flow ratios. The influence of the TiCl₄/BCl₃ gas flow ratio on the grain size and the deposition rate is discussed.

2. Experimental Methods

TiB₂ films were deposited on a high pure graphite substrate via CVD using a gas mixture of TiCl₄, BCl₃, and H₂. The overall reaction of the vapor deposition of TiB₂ is as follows [21]:



The 3D model diagram of the CVD reactor is illustrated in Figure 1. BCl₃, TiCl₄, and H₂ enter the deposition chamber through the air inlet at the bottom of the CVD reactor, however, H₂, BCl₃, and TiCl₄ were mixed in the gas mixing chamber before importing the deposition chamber. The graphite substrates were fixed on the sample stage. When the reaction begins, the rotating shaft drives the sample table to drive the graphite substrate to rotate. The rotating graphite substrate ensures the uniform films. A vacuum pump is connected to the air outlet for the aim of keeping the reactor in a vacuum during this entire sequence. The vacuum level was maintained at about 10 Pa during the reaction. During experimentation, TiCl₄ and BCl₃ were carried to the reactor by a heated line. The temperature of the TiCl₄ flow was 135 °C, and the BCl₃ flow was 12 °C. The heated TiCl₄ flow and BCl₃ flow were controlled by a mass flowmeter. Table 1 summarizes the field of deposition parameters.

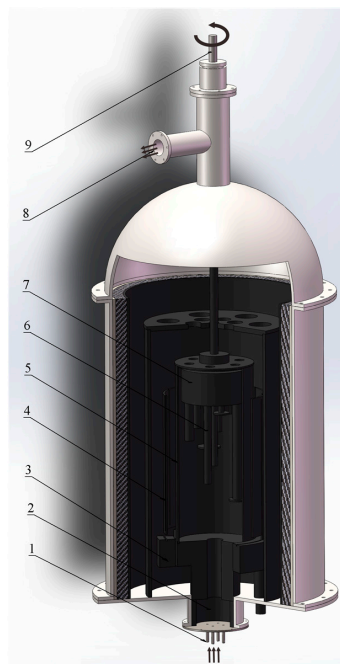


Figure 1. 3D model diagram of the CVD (chemical vapor deposition) reactor. (1) Air inlet; (2) gas mixing chamber; (3) electrode; (4) heating resistor; (5) deposition chamber; (6) high purity graphite substrate; (7) sample stage; (8) air outlet; (9) rotating shaft.

Table 1. Field of deposition parameters.

Substrate	Graphite
deposition temperature	1000 (°C)
deposition time	3 (h)
vacuum level	10 (Pa)
temperature of H ₂	25 (°C)
pressure of H ₂	0.06 (MPa)
flow rate of H ₂	0.9 (m ³ /h)
temperature of TiCl ₄	135 (°C)
pressure of TiCl ₄	0.1 (MPa)
flow rate of TiCl ₄	0.055, 0.11 (m ³ /h)
temperature of BCl ₃	12 (°C)
pressure of BCl ₃	0.1 (MPa)
flow rate of BCl ₃	0.085 (m ³ /h)

In this study, the deposition was carried out at 1000 °C. The deposition pressure was 10 Pa, and the deposition time was 3 h. In the experiment, the supply of hydrogen was excessive, and the BCl₃ flow rate was kept at 0.085 m³/h, then two types of specimens were synthesized at two TiCl₄ flow rate levels: 0.055 m³/h and 0.11 m³/h. When the TiCl₄ flow rate was 0.055 m³/h, the gas flow ratio of TiCl₄/BCl₃ (κ) was 0.5. At this point, κ was the stoichiometric TiCl₄/BCl₃ gas ratio. When the TiCl₄ flow rate was 0.11 m³/h, κ was 1. TiCl₄ was excessive in this situation. The microstructure and properties of these two types of films were investigated. In this way, the influence of the TiCl₄/BCl₃ gas flow ratio on the grain size and the deposition rate was studied.

The crystal phase of the films was determined by XRD (X'Pert Pro, PANalytical B.V., Almelo, The Netherlands). Special emphasis was put on the comparative analysis of micro structural characterization of these two types of films. In addition, SEM (Ultra Plus, ZEISS, Heidenheim, Germany), TEM (Tecnai G² 20, FEI, Hillsboro, OR, USA), and EDS (X-Max 50, OXFORD, Oxford, UK) were employed.

3. Results and Discussion

3.1. Structure, Morphology, and the Deposition Rate of Films

It was found that the oriented growth was related to the ratio of TiCl₄/BCl₃ from the orientation characteristics of the deposited layers investigated by X-ray diffraction shown in Figure 2 for a laser power 3 kW and laser scanning speed 2.5 mm/s. Figure 2a,b show the diffraction patterns of the deposits, which were prepared at $\kappa = 0.5$ and 1, respectively. In addition, the TiB₂ standard data from the Joint Committee on Powder Diffraction Standards (JCPDS) is shown in Figure 2c. X-ray diffraction (Figure 2a,b) indicated the presence of only TiB₂, with no unidentified peaks. Figure 2 also shows that the diffraction pattern of deposits corresponds well to the JCPDS standard for TiB₂. Furthermore, we found that the pattern intensity of the TiB₂ films, which were deposited at different gas ratios of TiCl₄/BCl₃ (Figure 2a,b), follows a similar trend. The intensity of the (100) peaks in Figure 2a,b are the highest of all peaks, respectively. However, there is an enhanced intensity at the (100) peaks compared with the standard pattern intensity shown in the JCPDS card NO. 85-2083 (Figure 2c). Furthermore, according to the XRD analysis, the relative intensity value of $R_{(100)/(101)}$ is 1.32 ± 0.01 (Figure 2a) and 1.28 ± 0.01 (Figure 2b). Similarly, the relative intensity of the standard pattern yields a $R_{(100)/(101)}$ value of 0.86 ± 0.01 (Figure 2c). Obviously, the $R_{(100)/(101)}$ values of the as-prepared TiB₂ films are greater than the standard values. Hence, all the as-prepared TiB₂ films have a preferred orientation along the (100) planes. These results are consistent with the work done by S.H. Lee [11], who reported that the film structure has a (100) preferred orientation when the film was deposited at a low RF power (200 W). The difference is that they prepared the TiB₂ film at a low temperature (250~400 °C) using a PACVD system.

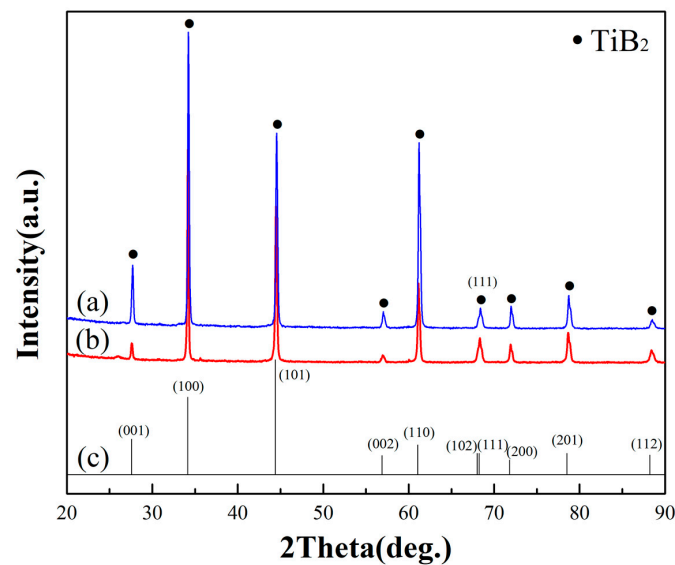


Figure 2. XRD (X-ray diffraction) patterns of TiB_2 deposits. (a) At a gas flow ratio of $\text{TiCl}_4/\text{BCl}_3 = 0.5$; (b) at a gas flow ratio of $\text{TiCl}_4/\text{BCl}_3 = 1$; (c) TiB_2 standard data from JCPDS (Joint Committee on Powder Diffraction Standards) card No. 85-2083.

The surfaces and cross sections of the TiB_2 films obtained by $\kappa = 0.5$ and 1 were observed by FESEM (Figures 3 and 4, respectively) with high voltages of 15 kV and magnifications of $5000\times$ and $20,000\times$. EDS results are also shown. An unsmooth surface can be observed on the films. The cross sections show a very compact and dense structure without any gaps. Figure 4 indicates the FESEM images and EDS results of the surface and cross section of TiB_2 films formed under the conditions of $\kappa = 1$. It can be discussed on different micrographs of the surfaces and cross sections by Figures 3 and 4. It was found that similar morphologies of the TiB_2 films were obtained by different gas flow ratios of $\text{TiCl}_4/\text{BCl}_3$. All TiB_2 films were found to have a typically columnar particle structure, and the columnar particles have a random orientation. This indicates that there was no distinct effect on morphologies by the $\text{TiCl}_4/\text{BCl}_3$ gas flow ratio in this experimentation. However, different film thicknesses were displayed in the cross sections (Figures 3 and 4). As shown in Figure 3, the thickness of the film deposited at $\kappa = 0.5$ for 3 h reached 15 microns. The thickness was 21 microns when κ was equal to 1 in Figure 4. Obviously, a thicker TiB_2 film was obtained by a greater $\text{TiCl}_4/\text{BCl}_3$ gas flow ratio that goes beyond the stoichiometric $\text{TiCl}_4/\text{BCl}_3$ gas flow ratio. In other words, the film deposited faster when TiCl_4 was excessive.

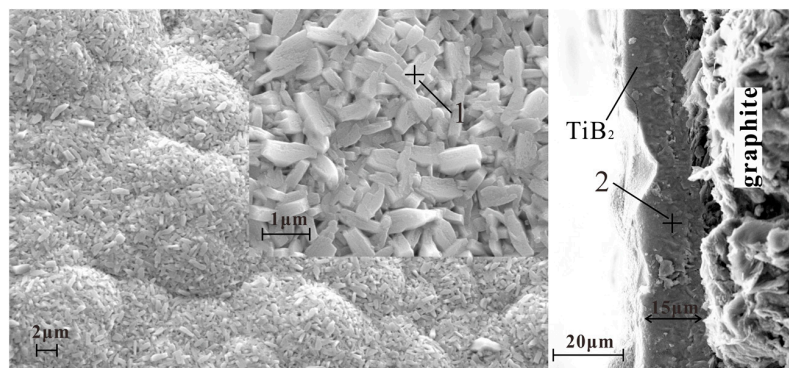


Figure 3. Cont.

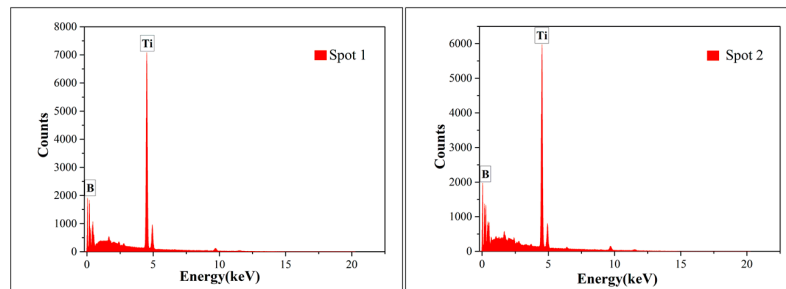


Figure 3. SEM (scanning electron microscopy) images and EDS (energy dispersive spectroscopy) results of the surface and cross section of the TiB_2 film formed under the condition of a $\text{TiCl}_4/\text{BCl}_3$ gas flow ratio of 0.5.

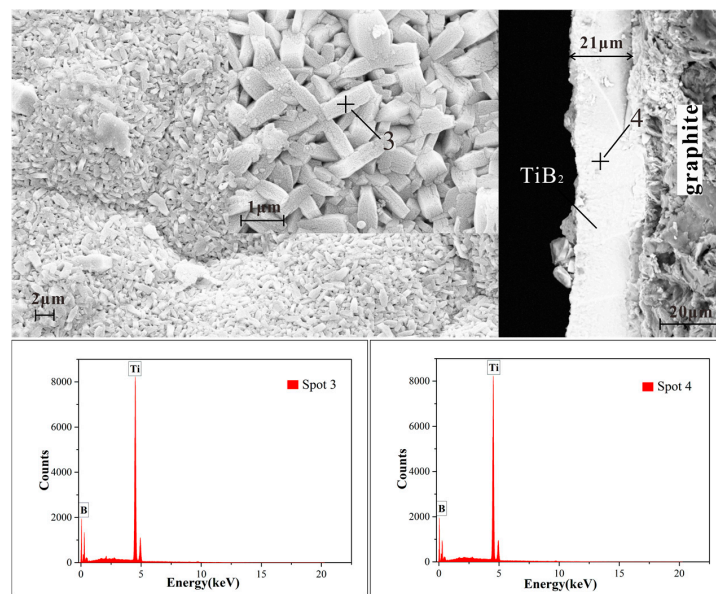


Figure 4. SEM images and EDS results of the surface and cross section of the TiB_2 film formed under the condition of a $\text{TiCl}_4/\text{BCl}_3$ gas flow ratio of 1.

Table 2 shows the compositional analysis results of Spot 1, Spot 2, Spot 3, and Spot 4, analyzed via EDS. The Ti/B ratio of the deposit approached the stoichiometric value of 0.5 when the gas flow ratio of $\text{TiCl}_4/\text{BCl}_3$ was increased. According to the CVD phase diagram of the Ti–B–H–Cl system which was calculated by Randich and Gerlach [23], the formability of TiB_2 relies on the distance between the process tie line and the phase boundary of the TiB_2 + gas and the gas phases. A boron rich TiB_x film was deposited when the BCl_3 concentration was high, because the process tie line went through the region of the B + TiB_2 + gas phase. Therefore, at a low $\text{TiCl}_4/\text{BCl}_3$ gas ratio, boron rich TiB_x films were formed instead of TiB_2 .

Table 2. The EDS (energy dispersive spectroscopy) analysis results of different regions of samples in Figures 3 and 4.

Spot No.	Element	wt %	atom %	Ti/B Atom Ratio
1	B	38.01	73.15	0.367
	Ti	61.92	26.85	
2	B	37.68	72.84	0.373
	Ti	62.32	27.16	
3	B	33.54	69.10	0.447
	Ti	66.46	30.90	
4	B	33.23	68.80	0.453
	Ti	66.70	31.20	

3.2. Grain Size of the Films

Many scholars [6,11,19] have researched the influence of deposition temperature on grain size, and they all agreed that the grain size increases with increasing temperature. Indeed, this conclusion is in good agreement with the kinetic theory of CVD [24]. Comparatively few research groups have studied the effect of $\text{TiCl}_4/\text{BCl}_3$ gas flow ratio on grain size.

The grain size of the TiB_2 films was calculated by XRD patterns of TiB_2 films (Figure 2) using the Scherrer formula. The grain size was 58 ± 3 nm when the TiB_2 film was deposited at a stoichiometric $\text{TiCl}_4/\text{BCl}_3$ gas ratio of 0.5, and the grain size was 69 ± 3 nm when $\kappa = 1$. Hence, all the as-deposited TiB_2 films had a nano-sized grain structure. Figures 5 and 6 show TEM images of the films formed under different gas flow ratios of $\text{TiCl}_4/\text{BCl}_3$. Bright nano-sized shapes can be observed in the dark field images (Figures 5a and 6a), wherein it can be seen that the common shapes of the grains reveal a columnar and that the grain size is at the nano scale. The grain size is also easily observed. The grains are larger in Figure 6a than in Figure 5a. Analysis of the selected-area electron diffraction (SAED) pattern (Figures 5b and 6b) revealed only the presence of TiB_2 . The average grain size in the plan view (dark field image) was estimated to be at the nano scale and to cause continuous rings in the diffraction pattern (as shown in Figures 5b and 6b). However, the diffraction ring, as shown in Figures 5b and 6b, is a little bit different. In Figure 5b, the diffraction ring is smooth and continuous. In contrast, the ring intensities in Figure 6b do not show uniform continuity, and there are bright spots on the circular rings. This is because the grain of the selected area in Figure 6a is larger. Thus, the SAED pattern further reveals that the grain size in Figure 6a is greater than that in Figure 5a. These SAED results correspond to Figures 5a and 6a. As a result, TEM investigations indicate that all as-prepared TiB_2 films are nanocrystalline and that the grain size is different under various $\text{TiCl}_4/\text{BCl}_3$ gas flow ratios. Obviously, the TEM results are in good agreement with the results calculated by the Scherrer formula. Therefore, $\text{TiCl}_4/\text{BCl}_3$ gas flow ratio has a certain impact on the grain size of as-prepared TiB_2 films via CVD. The grain size of TiB_2 films deposited at $\kappa = 1$ is greater than that of other films obtained under conditions where $\kappa = 0.5$.

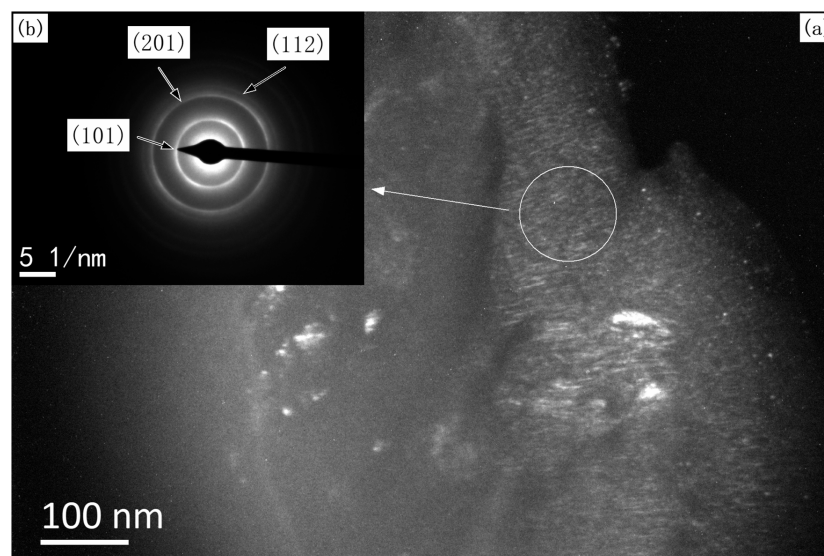


Figure 5. TEM images of the synthesized TiB_2 film formed by CVD with a $\text{TiCl}_4/\text{BCl}_3$ gas flow ratio of 0.5: (a) dark field image, (b) corresponding selected-area electron diffraction pattern.

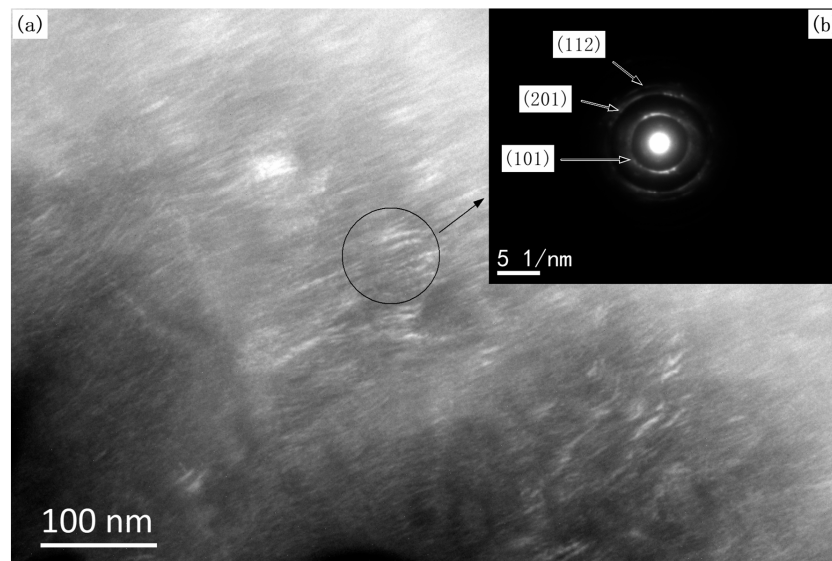


Figure 6. TEM images of the synthesized TiB_2 film formed by CVD with a $\text{TiCl}_4/\text{BCl}_3$ gas flow ratio of 1: (a) dark field image, (b) corresponding selected-area electron diffraction pattern.

4. Conclusions

TiB_2 was prepared via the vapor-phase reaction of TiCl_4 , BCl_3 , and H_2 on a high pure graphite substrate. The following information was obtained:

1. TiB_2 could be deposited at 1000 °C and 10 Pa by a CVD system. All deposits obtained under the condition of excessive hydrogen and different $\text{TiCl}_4/\text{BCl}_3$ gas flow ratios (1/2 and 1/1) were TiB_2 . Other impurity phases such as TiB were not found.
2. These TiB_2 films are nanocrystalline with a grain size in the range of 60 nm. All of the TiB_2 films were typically columnar particles structure, and the columnar particles have a random orientation.
3. X-ray diffraction indicated that all of the as-synthesized TiB_2 films have a preferential orientation growth in the (100) direction.
4. The $\text{TiCl}_4/\text{BCl}_3$ gas flow ratio has a certain impact on deposition rate and grain size, but these variations in the gas flow ratio of $\text{TiCl}_4/\text{BCl}_3$ did not appear to influence the preferred orientation of the deposits. The deposition rate is faster when using a greater $\text{TiCl}_4/\text{BCl}_3$ gas flow ratio, which in this case was 1/1. Meanwhile, when we provided a stoichiometric $\text{TiCl}_4/\text{BCl}_3$ gas ratio of 1/2, the grain size of the as-deposited TiB_2 film was smaller.

Acknowledgments: The authors are grateful for the financial support of the Foundation Committee of the National Nature of China (No. 50904017). Their support enabled us to complete this work.

Author Contributions: Xiaoxiao Huang planned and performed the experiments, analyzed the experimental data, and wrote the manuscript. Shuchen Sun directed and guided the research and extensively provided help for editing the manuscript. Ganfeng Tu provided useful insights into the manuscript. Shuaidan Lu took the TEM images. Kuanhe Li and Xiaoping Zhu prepared the TEM samples. All authors contributed in discussion and preparation of the manuscript.

Conflicts of Interest: The authors declare no conflict of interest.

References

1. Schalk, N.; Keckes, J.; Czettel, C.; Burghammer, M.; Penoy, M.; Michotte, C.; Mitterer, C. Investigation of the origin of compressive residual stress in CVD TiB_2 hard coatings using synchrotron X-ray nanodiffraction. *Surf. Coat. Technol.* **2014**, *258*, 121–126. [[CrossRef](#)]
2. Raju, G.B.; Basu, B. Development of high temperature TiB_2 -based ceramics. *Key Eng. Mater.* **2009**, *395*, 89–124. [[CrossRef](#)]

3. Shimada, S.; Takahashi, M.; Kiyono, H.; Tsujino, J. Coatings and microstructures of monolithic TiB₂ films and double layer and composite TiCN/TiB₂ films from alkoxide solutions by thermal plasma CVD. *Thin Solid Films* **2008**, *516*, 6616–6621. [[CrossRef](#)]
4. Tang, W.-M.; Zheng, Z.-X.; Wu, Y.-C.; Wang, J.-M.; Lü, J.; Liu, J.-W. Synthesis of TiB₂ nanocrystalline powder by mechanical alloying. *Trans. Nonferrous Met. Soc. China* **2006**, *16*, 613–617. [[CrossRef](#)]
5. Berger, M.; Coronel, E.; Olsson, E. Microstructure of d.c. Magnetron sputtered TiB₂ coatings. *Surf. Coat. Technol.* **2004**, *185*, 240–244. [[CrossRef](#)]
6. Pfohl, C.; Bulak, A.; Rie, K.T. Development of titanium diboride coatings deposited by PACVD. *Surf. Coat. Technol.* **2000**, *131*, 141–146. [[CrossRef](#)]
7. Martin, C.; Cales, B.; Vivier, P.; Mathieu, P. Electrical discharge machinable ceramic composites. *Mater. Sci. Eng. A* **1989**, *109*, 351–356. [[CrossRef](#)]
8. Tenny, V.; Finch, C.; Yust, C.; Clark, G. Structure-property correlations for TiB₂-based ceramics densified using active liquid metals. In *Science of Hard Materials*; Springer: Boston, MA, USA, 1983; pp. 891–909, ISBN 978-1-4684-4319-6.
9. Ferber, M.K.; Becher, P.F.; Finch, C.B. Effect of microstructure on the properties of TiB₂ ceramics. *J. Am. Ceram. Soc.* **1983**, *66*, C-2–C-3. [[CrossRef](#)]
10. Subramanian, C.; Murthy, T.S.R.C.; Suri, A.K. Synthesis and consolidation of titanium diboride. *Int. J. Refract. Met. Hard Mater.* **2007**, *25*, 345–350. [[CrossRef](#)]
11. Lee, S.H.; Nam, K.H.; Hong, S.C.; Lee, J.J. Low temperature deposition of TiB₂ by inductively coupled plasma assisted CVD. *Surf. Coat. Technol.* **2007**, *201*, 5211–5215. [[CrossRef](#)]
12. Elders, J.; van Voorst, J.D.W. Laser-induced chemical vapor deposition of titanium diboride. *Appl. Surf. Sci.* **1992**, *54*, 135–140. [[CrossRef](#)]
13. Sun, L.; Gao, Y.; Xiao, B.; Li, Y.; Wang, G. Anisotropic elastic and thermal properties of titanium borides by first-principles calculations. *J. Alloys Compd.* **2013**, *579*, 457–467. [[CrossRef](#)]
14. Wang, H.; Sun, S.; Wang, D.; Tu, G. Characterization of the structure of TiB₂/TiC composites prepared via mechanical alloying and subsequent pressureless sintering. *Powder Technol.* **2012**, *217*, 340–346. [[CrossRef](#)]
15. Vallauri, D.; Atías Adrián, I.C.; Chrysanthou, A. TiC–TiB₂ composites: A review of phase relationships, processing and properties. *J. Eur. Ceram. Soc.* **2008**, *28*, 1697–1713. [[CrossRef](#)]
16. Jeitschko, W.; Pöttgen, R.; Hoffman, R. Structural chemistry of hard materials. In *Handbook of Ceramic Hard Materials*, 1st ed.; Wiley-VCH: New York, NY, USA, 2008; pp. 10–11, ISBN 9783527618217.
17. Batanov, G.M.; Berezhetzkaya, N.K.; Borzosekov, V.D.; Iskhakova, L.D.; Kolik, L.V.; Konchekov, E.M.; Letunov, A.A.; Malakhov, D.V.; Milovich, F.O.; Obratsova, E.A.; et al. Application of microwave discharge for the synthesis of TiB₂ and bn nano- and microcrystals in a mixture of Ti-B powders in a nitrogen atmosphere. *Plasma Phys. Rep.* **2013**, *39*, 843–848. [[CrossRef](#)]
18. Kang, S.H.; Kim, D.J. Synthesis of nano-titanium diboride powders by carbothermal reduction. *J. Eur. Ceram. Soc.* **2007**, *27*, 715–718. [[CrossRef](#)]
19. Caputo, A.J. Chemical vapor deposition of erosion-resistant TiB₂ coatings. *J. Electrochem. Soc.* **1985**, *132*. [[CrossRef](#)]
20. Pierson, H.O.; Randich, E.; Mattox, D.M. The chemical vapor deposition of TiB₂ on graphite. *J. Less Common Met.* **1979**, *67*, 381–388. [[CrossRef](#)]
21. Takahashi, T.; Kamiya, H. Chemical vapor deposition of titanium diboride. *J. Cryst. Growth* **1974**, *26*, 203–209. [[CrossRef](#)]
22. Williams, L.M. Plasma enhanced chemical vapor deposition of titanium diboride films. *Appl. Phys. Lett.* **1985**, *46*, 43–45. [[CrossRef](#)]
23. Randich, E.; Gerlach, T.M. The calculation and use of chemical vapor deposition phase diagrams with applications to the Ti–B–Cl–H system between 1200 and 800 K. *Thin Solid Films* **1981**, *75*, 271–291. [[CrossRef](#)]
24. Pierson, H.O. Fundamentals of Chemical Vapor Deposition. In *Handbook of Chemical Vapor Deposition: Principles, Technology and Applications*, 2nd ed.; William Andrew: New York, NY, USA, 1999; pp. 43–63, ISBN 0815517432.

